Self-organised stripe domains and elliptical skyrmion bubbles in ultra-thin epitaxial Au0.67Pt0.33/Co/W(110) films

Lorenzo Camosi, José Peña-Garcia, Olivier Fruchart, Tevfik Onur Menteş, Stefania Pizzini, Andrea Locatelli, Francesca Genuzio, Justin M. Shaw, Hans T. Nembach, Jan Vogel

New Journal of Physics
The open access journal at the forefront of physics

Deutsche Physikalische Gesellschaft DPG
IOP Institute of Physics

Published in partnership with: Deutsche Physikalische Gesellschaft and the Institute of Physics

OPEN ACCESS

RECEIVED
8 October 2020

REVISED
22 December 2020

ACCEPTED FOR PUBLICATION
14 January 2021

PUBLISHED
29 January 2021

PAPER

Self-organised stripe domains and elliptical skyrmion bubbles in ultra-thin epitaxial $Au_{0.67}Pt_{0.33}$/Co/W(110) films

Lorenzo Camosi[1,6,7], Jose Peña Garcia[1,7], Olivier Fruchart[2], Stefania Pizzini[1], Andrea Locatelli[3], Tevfik Onur Menteş[3], Francesca Genuzio[3], Justin M Shaw[4], Hans T Nembach[4,5] and Jan Vogel[1,*]

[1] Univ. Grenoble Alpes, CNRS, Institut Néel, 38054 Grenoble, France
[2] Univ. Grenoble Alpes, CNRS, CEA, SPINTEC, 38042 Grenoble, France
[3] Elettra-Sincrotrone Trieste S.C.p.A, S.S 14-km 163.5 in AREA Science Park 34149 Basovizza, Trieste, Italy
[4] Quantum Electromagnetics Division, National Institute of Standards and Technology, Boulder, CO 80305, United States of America
[5] JILA, University of Colorado, Boulder, CO 80309, United States of America
[6] Present address: ICN2, Univ. Autonomous of Barcelona, Barcelona, 08193, Spain.
[7] The first two authors contributed equally to this work.
[*] Author to whom any correspondence should be addressed.

E-mail: lorenzo.camosi@gmail.com, jose.pena-garcia@neel.cnrs.fr and jan.vogel@neel.cnrs.fr

Keywords: Dzyaloshinskii–Moriya interaction, magnetic skyrmions, epitaxial thin films

Supplementary material for this article is available online

Abstract

We studied the symmetry of magnetic properties and the resulting magnetic textures in ultra-thin epitaxial $Au_{0.67}Pt_{0.33}$/Co/W(110), a model system exhibiting perpendicular magnetic anisotropy and interface Dzyaloshinskii–Moriya interaction (DMI). As a peculiar feature, the C_{2v} crystal symmetry induced by the Co/W interface results in an additional uniaxial in-plane magnetic anisotropy in the cobalt layer. Photo-emission electron microscopy with magnetic sensitivity reveals the formation of self-organised magnetic stripe domains oriented parallel to the hard in-plane magnetisation axis. We attribute this behavior to the lower domain wall energy when oriented along this axis, where both the DMI and the in-plane magnetic anisotropy favor a Néel domain wall configuration. The anisotropic domain wall energy also leads to the formation of elliptical skyrmion bubbles under a weak out-of-plane magnetic field.

1. Introduction

Chiral magnetic spin textures are interesting candidates for future applications in data storage and spintronics [1]. In perpendicularly magnetised ultra-thin films, chirality may be induced by the Dzyaloshinskii–Moriya interaction (DMI) [2, 3]. The DMI is a chiral anti-symmetric exchange interaction, which may exist in systems with a lack of structural inversion symmetry and a strong spin–orbit coupling. In ultra-thin magnetic films, the conditions that can lead to an interfacial DMI are satisfied if the two interfaces are different (inversion symmetry breaking) and is increased if at least one of the interfaces contains a heavy metal such as Pt or W (strong spin–orbit coupling).

An appropriate balance between the DMI, Heisenberg exchange interaction, dipolar interactions and magnetocrystalline anisotropy (MCA) can lead to the stabilisation of chiral Néel domain walls (DW) and Néel-type skyrmions [4, 5]. Skyrmions are chiral whirling magnetic configurations with a non-trivial topology [6], which have been theoretically investigated [7] and experimentally observed in bulk systems with B20 symmetry [8], and, in a metastable state, in ultra-thin magnetic films [9–11]. Until now, most thin film magnetic systems hosting skyrmions and skyrmion bubbles [12] at room temperature were prepared by sputter deposition [10, 11, 13, 14], leading to polycrystalline systems with isotropic properties within the film plane. These systems display an in-plane circular symmetry, so that DW and skyrmions show isotropic properties.

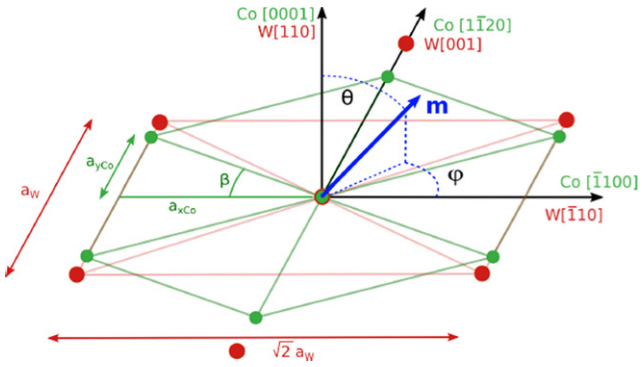

Figure 1. Overlay of the W(110) and the strained Co(0001) surfaces with the Nishiyama–Wasserman epitaxial relationship [21, 22]. Red and green dots represent tungsten and cobalt atoms, respectively. The geometry and notation used to describe the magnetisation **m** in polar coordinates (θ, φ) in the W bcc(110) crystal frame are also illustrated.

In epitaxial systems, however, the symmetry of the magnetic interactions reflects the crystal symmetry of the magnetic crystal and its interfaces [15–17]. In systems with C_{2v} symmetry, for example, uniaxial and/or biaxial in-plane magnetic anisotropies can occur [18], whereas the DMI may have different strength and sign along two perpendicular in-plane directions [19]. We recently confirmed experimentally such anisotropic properties in epitaxial Au/Co/W(110) thin films with C_{2v} symmetry, where in addition to an out-of-plane easy magnetisation axis, a uniaxial in-plane anisotropy and a strongly anisotropic DMI were observed [20].

In the present work, we investigate the influence of the out-of-plane and in-plane anisotropies on magnetic textures such as DW and skyrmion bubbles in an epitaxial AuPt/Co/W(110) film with C_{2v} symmetry. The introduction of Pt in the top layer is expected to strongly increase the DMI with respect to the Au/Co/W(110) system studied previously, while reducing the out-of-plane MCA. The system is grown using pulsed laser deposition (PLD) and the crystal symmetry is studied *in situ* with reflection high energy electron diffraction (RHEED). The magnetic properties are investigated with a vibrating-sample magnetometer based on a superconducting quantum interference device (VSM-SQUID), Kerr magnetometry, Kerr microscopy and Brillouin light scattering (BLS). Chiral DW and skyrmions are studied theoretically using micromagnetic simulations and are observed experimentally using photo-emission electron microscopy combined with x-ray magnetic circular dichroism (XMCD-PEEM). These measurements show that the anisotropic magnetic properties lead to the formation of magnetic stripe domains spontaneously oriented along the in-plane hard magnetisation axis, which transform into elliptical skyrmion bubbles upon application of a small out-of-plane magnetic field.

2. Sample growth

The $Au_{0.67}Pt_{0.33}$/Co/W(110) stack was grown in a PLD system under ultra high vacuum conditions ($P \approx 10^{-9}$ Pa). A 10 Hz-pulsed Nd-YAG laser with pulse length ≈10 ns and doubled frequency ($\lambda = 532$ nm) was used. The deposition chamber was equipped with a 10 kV RHEED. The substrates were commercial $Al_2O_3(11\bar{2}0)$ single crystals. Prior to the growth, the deposition rate was calibrated using a quartz crystal microbalance.

The growth process is similar to the one described in our previous work [20]. First, 0.8 nm of bcc-Mo(110) was deposited at room temperature, followed by the deposition at 370 K of 10 nm bcc-W(110). After annealing at 1070 K for 1 h, the buffer layer showed a high crystal quality as deduced from the *in situ* RHEED 1 × 1 diffraction pattern and the ex-situ $\theta/2\theta$ x-ray diffraction patterns, where Kiessig fringes with many orders were observed (see supplemental material (http://stacks.iop.org/JPCM/23/013020/mmedia)). A wedge of Co with a thickness ranging from 2 to 4 monolayers (ML) (1 monolayer ≈ 0.2 nm) was deposited with the help of a computer-controlled mask moving in front of the sample. The sample was progressively warmed up from room temperature to 350 K while the Co thickness increased [20]. The Co(0001) film grows on the W bcc(110) surface following the Nishiyama–Wassermann orientation [21, 22], i.e., with a unique epitaxial relationship with the Co[1100]-direction parallel to W[$\bar{1}$10] and the Co[1$\bar{1}$20] parallel to W[001] (figure 1). These epitaxial relationships are confirmed by RHEED, where it is observed that the Co grows pseudomorphically along W[$\bar{1}$10] and relaxed along W[001] (see supplemental material). This particular growth mode induces a C_{2v} symmetry in the Co/W system. In the following, we use the W(110) crystallographic directions as the reference frame (figure 1).

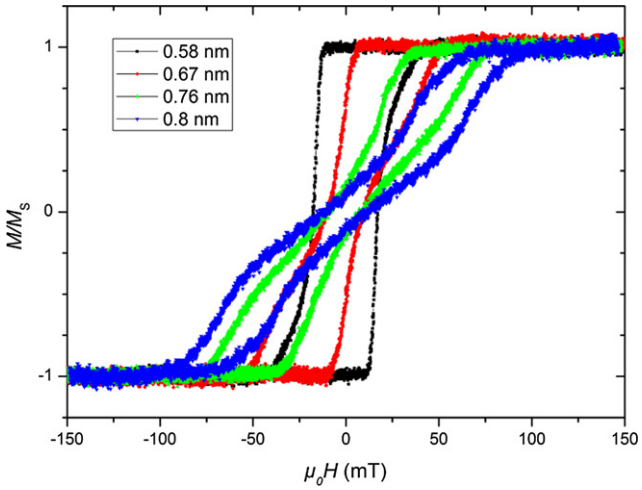

Figure 2. Hysteresis loops obtained by focused polar Kerr measurements for different Co thicknesses.

Finally, a solid solution of $Au_{0.67}$–$Pt_{0.33}$ is deposited at room temperature. A solid solution allows a continuous variation of the chemical composition and lattice parameter, which is not possible for pure elements. The solid solution is obtained by alternating seven times the deposition of 0.66 ML of Au and of 0.33 ML of Pt, up to a total thickness of 7 MLs, with the aim to promote the mixture of the two elements at the atomic level and to avoid the formation of misfit dislocations [23]. The deposition is performed at a constant rate of 1 ML/300 s. This proportion of Pt corresponds to an α-phase made of fcc-(111) (Au) + (Pt) [24], which is likely to result in averaged properties of the two pure metals (crystal lattice constant, induced MCA and DMI).

3. Magnetic characterisation

We used focused Kerr magnetometry to study the magnetic properties for different Co thicknesses. The polar Kerr cycles were measured as a function of an out-of-plane magnetic field. Figure 2 shows the hysteresis loops measured at different locations along the wedge, corresponding to different Co thicknesses. For $t_{Co} \approx 0.58$ nm a square hysteresis loop is obtained, which indicates that the sample magnetisation is fully saturated at remanence. With increasing Co thickness, the decrease in the effective anisotropy K_{out} leads to a slanted loop, in agreement with a multi-domain state at zero field. The ratio M/M_S at zero field decreases as t_{Co} increases from ≈0.67 nm to ≈0.8 nm where the magnetisation is close to the spin-reorientation transition, and the remanence is close to zero. The spontaneous magnetisation $M_s = 1.15 \pm 0.10$ MA m^{-1} was extracted from VSM-SQUID measurements for a Co thickness of 0.8 nm.

The C_{2v} symmetry, resulting from the epitaxial growth on W(110), induces an in-plane magnetic anisotropy energy density (E_{MAE}) in the system, in addition to the uniaxial out-of-plane anisotropy induced by the AuPt/Co interface. E_{MAE} may be expressed in the second-order approximation using spherical coordinates (θ, φ) [see figure 1(b)]

$$E_{MAE}(\theta, \varphi) = -K_{out} \cos^2 \theta - K_{in} \sin^2 \theta \cos^2 \varphi \quad (1)$$

where K_{out} is the effective out-of-plane anisotropy coefficient, defined as the difference in energy between the magnetisation oriented along the hard in-plane direction and oriented perpendicular to the film plane. It can be expressed as $K_{out} = K_u$–K_d with K_u being the out-of-plane magneto-crystalline anisotropy constant and $K_d = \frac{1}{2}\mu_0 M_s^2$ the dipolar energy density. Finally, K_{in} is the in-plane anisotropy coefficient, the difference in energy for the magnetisation oriented along the in-plane hard and easy axes. VSM-SQUID hysteresis loops with a magnetic field along the main in-plane crystallographic axes were also recorded. A smaller saturation field was required for a magnetic field applied along W[$\bar{1}$10] than along W[001]. Therefore, this confirms the Co axis parallel to W[$\bar{1}$10] as the in-plane easy axis [18].

We performed BLS spectroscopy in the Damon–Eshbach configuration [25], for a Co thickness of 0.8 nm, in order to determine K_{in}, K_{out} and the DMI parameters along the [001] and [$\bar{1}$10] directions. The magnetisation is consecutively saturated along the hard and easy in-plane magnetisation axes of the film by an external magnetic field. The spin waves (SW) propagating along the direction perpendicular to this field are probed by a laser with a well-defined wave vector k_{SW}. Due to the DMI, the SWs involved in the

Table 1. BLS measurements for Au/Co(0.65 nm)/W (from reference [20]) and $Au_{0.67}Pt_{0.33}$/Co(0.8 nm)/W.

System	Au/Co/W [20]	$Au_{0.67}Pt_{0.33}$/Co/W
$D_x \times t_{Co}$ (pJ m^{-1})	0.29 ± 0.03	0.74 ± 0.1
$D_y \times t_{Co}$ (pJ m^{-1})	0.12 ± 0.02	0.79 ± 0.1
K_u (kJ m^{-3})	1100 ± 400	970 ± 100
K_{in} (kJ m^{-3})	136 ± 6	94 ± 9

scattering phenomena propagating along opposite directions have different energies. By measuring the spin-wave frequency for positive and negative field polarity, we obtain the frequency-shift $\Delta f = \frac{f(+H)-f(-H)}{2} = \frac{g\mu_B}{h}\frac{2D}{M_s}k_{SW}$ with g the Landé factor, μ_B the Bohr magneton, h Planck's constant, D the micromagnetic DMI constant in J m^{-2}, and M_s the spontaneous magnetisation in A m^{-1} [26–29]. In this experiment, $k_{SW} = 16.7\ \mu m^{-1}$ and $g = 2.17$ [28].

The BLS results obtained for $Au_{0.67}Pt_{0.33}$/Co(0.8 nm)/W are compared with our previous results for Au/Co(0.65 nm)/W [20] in table 1. In the following, we will indicate with x the bcc[$\bar{1}$10] direction (in-plane easy axis) and with y the bcc[001] direction (in-plane hard axis). Since the DMI is mainly an interfacial effect, D_x and D_y have been multiplied by t_{Co} to take the difference in Co thickness of the two samples into account. The data show that along both in-plane directions the DMI strongly increases with the addition of Pt, with respect to Au/Co/W, while the in-plane anisotropy K_{in} decreases. Note that the error in the value of D mainly originates from the uncertainty in M_s.

The inclusion of Pt in the top layer strongly increases the DMI strength due to the stronger DMI at the Pt/Co interface [30], but does not affect the chirality. The measured effective DMI of the trilayer systems is the total contribution from both the top and bottom Co interfaces. It was reported by Ma *et al* [31] that the DMI at the Co/Au interface is negative, as is also the case for Co/Pt, and stronger than that of Co/W, which is positive. In both Au/Co/W and Pt/Co/W trilayers the DMI at the two interfaces thus induces a right-handed chirality, and the positive DMI we measure in our system is in agreement with the literature. While we observed a strong anisotropy of the DMI in Au/Co/W, with the largest DMI along the in-plane easy axis, a much smaller anisotropy is found in $Au_{0.67}Pt_{0.33}$/Co/W with the largest DMI along the in-plane hard axis. This may arise from the large contribution to the DMI of the $Au_{0.67}Pt_{0.33}$/Co interface, which may be isotropic or even show an anisotropy opposite to the one at the Co/W interface.

4. Anisotropic magnetic textures

4.1. One-dimensional model

In this subsection, we discuss phenomenologically the DW configuration along the in-plane easy and hard axes, and the predictions that a one-dimensional (1D) micromagnetic model allows us to make in the case of perpendicular magnetic anisotropy.

In thin film systems with reduced symmetry the competition between the DMI and the MCA is expected to induce an anisotropic magnetic configuration of the DWs [16]. We can expect that for DW oriented along the W[001] (in-plane hard axis, y) direction, both the in-plane anisotropy and the DMI are promoting a Néel configuration, which is chiral because of the DMI (figure 3). For DW oriented along the W[$\bar{1}$10] (in-plane easy axis, x) direction, the DMI is promoting a chiral Néel configuration while the in-plane anisotropy promotes a non-chiral Bloch configuration (figure 3), leading to an intermediate angle φ (or $\pi-\varphi$), in between a Bloch and a Néel wall [16], with φ depending on the relative strength of K_{in} and D. In the phenomenological sketch of figure 3 both the DMI and the magnetic anisotropy are represented as effective in-plane fields.

Considering a Bloch profile as an ansatz [4], we can express the domain wall areal density of energy along the two directions x and y as:

$$\sigma_x = \frac{2A}{\Delta} + 2K_{out}\Delta - 2K_{in}\Delta\cos^2\varphi - \pi D_y \sin\varphi \quad (2)$$

$$\sigma_y = \frac{2A}{\Delta} + 2K_{out}\Delta - 2K_{in}\Delta\cos^2\varphi - \pi D_x \cos\varphi \quad (3)$$

where A is the exchange stiffness, K_{out} and K_{in} are the anisotropy constants defined in equation (1), and Δ is the domain wall width parameter. Finally, note that the magnetostatic energy term, which favors the Bloch wall, has been neglected in order to preserve analytical expressions. However, as discussed in the supplemental material, the numerical solution including the magnetostatic energy term does not change the main results presented here.

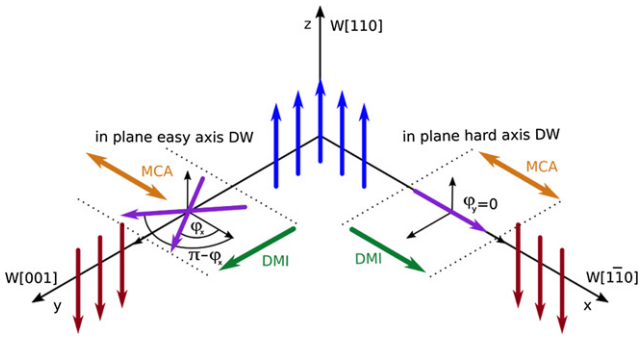

Figure 3. Sketch of the possible configurations for DW oriented along the in-plane hard axis and the in-plane easy axis. Red, blue and purple arrows: magnetisation direction. Orange arrows: effective in-plane anisotropy field direction. Green arrows: effective DMI field direction.

The minimisation of equations (2) and (3) with respect to Δ and φ allows finding the equilibrium domain wall width parameters Δ_x and Δ_y and the angles φ_x and φ_y between the magnetisation direction and $[\bar{1}10]$ along x and y, respectively:

$$\Delta_x = \sqrt{\frac{A}{K_{\text{out}} - K_{\text{in}} \cos^2 \varphi_x}} \tag{4}$$

$$\Delta_y = \sqrt{\frac{A}{K_{\text{out}} - K_{\text{in}}}} \tag{5}$$

$$\varphi_x = \arctan\left(\xi \sqrt{\frac{\kappa - 1}{1 - \xi^2}}\right) \tag{6}$$

$$\varphi_y = 0 \tag{7}$$

where $\xi = \frac{\pi D_y}{4\sqrt{AK_{\text{in}}}}$ and $\kappa = K_{\text{out}}/K_{\text{in}}$. Both quantities are dimensionless. Note that in equation (6), φ_x depends on the thickness of the ferromagnetic layer, since the in-plane magnetic anisotropy is a volume effect due to strain [18], whereas the DMI in this system is an interface effect. For very small thickness the DMI dominates, promoting a Néel configuration. However, when the strength of the DMI decreases becoming comparable to the in-plane anisotropy, an intermediate Bloch–Néel configuration is stabilised.

It can be seen that, in DW oriented along the in-plane easy axis, the terms due to K_{in} and to D_y in the domain wall areal energy density σ_x (equation (2)) cannot be minimised for the same angle φ, while in σ_y (equation (3) an angle $\varphi = 0$ minimises both terms. Depending on the parameters, the domain wall energy density for DW oriented along y can thus be considerably smaller than for DW oriented along x. Introducing the parameters in table 1 determined by VSM and BLS for a thickness of 0.8 nm, and considering an exchange interaction of 16 pJ m^{-1} [32], we find that for DW oriented along the y direction, $\varphi = 0°$ and $\pi\Delta_y = 51 \pm 10$ nm; for DW oriented along x, we expect that $\varphi = 34°$ with $\pi\Delta_x = 46 \pm 10$ nm. For the domain wall energy densities, we find $\sigma_x = 2.7 \pm 0.5$ mJ m^{-2} and $\sigma_y = 0.5 \pm 0.2$ mJ m^{-2}.

4.2. Domain structure and domain wall configuration

In order to determine experimentally the domain structure and the domain wall configuration in the $Au_{0.67}Pt_{0.33}$/Co/W system, we used XMCD-PEEM at the Nanospectroscopy beamline of the Elettra synchrotron (Trieste). The local magnetic contrast in this technique is proportional to the projection of the magnetisation on the x-ray beam direction. In our experiment, the x-ray beam is oriented with a grazing incidence of 16° with respect to the sample surface, implying that we are about 3 times more sensitive to the in-plane component of the magnetisation than to the out-of-plane component. Together with the high lateral spatial resolution (down to 25 nm) and the high sensitivity, this technique is particularly suited to study the domain wall configuration in our thin film system.

The domain configuration for Co thicknesses between 0.6 and 0.7 nm is shown in figure 4. The images were recorded at room temperature at zero magnetic field, with the incoming x-ray beam parallel to the W[001] direction. Dark and bright gray contrast corresponds to the magnetisation pointing up and down, respectively, perpendicular to the film plane. As expected from the 1D model, the stripe domains are almost uniquely oriented close to the W[001] direction, as a direct consequence of the lower domain wall energy for DW oriented along [001] than along $[\bar{1}10]$. The stripe domain width sharply decreases with increasing Co thickness [figures 4(a) and (b)]. This width is determined by the competition between the dipolar

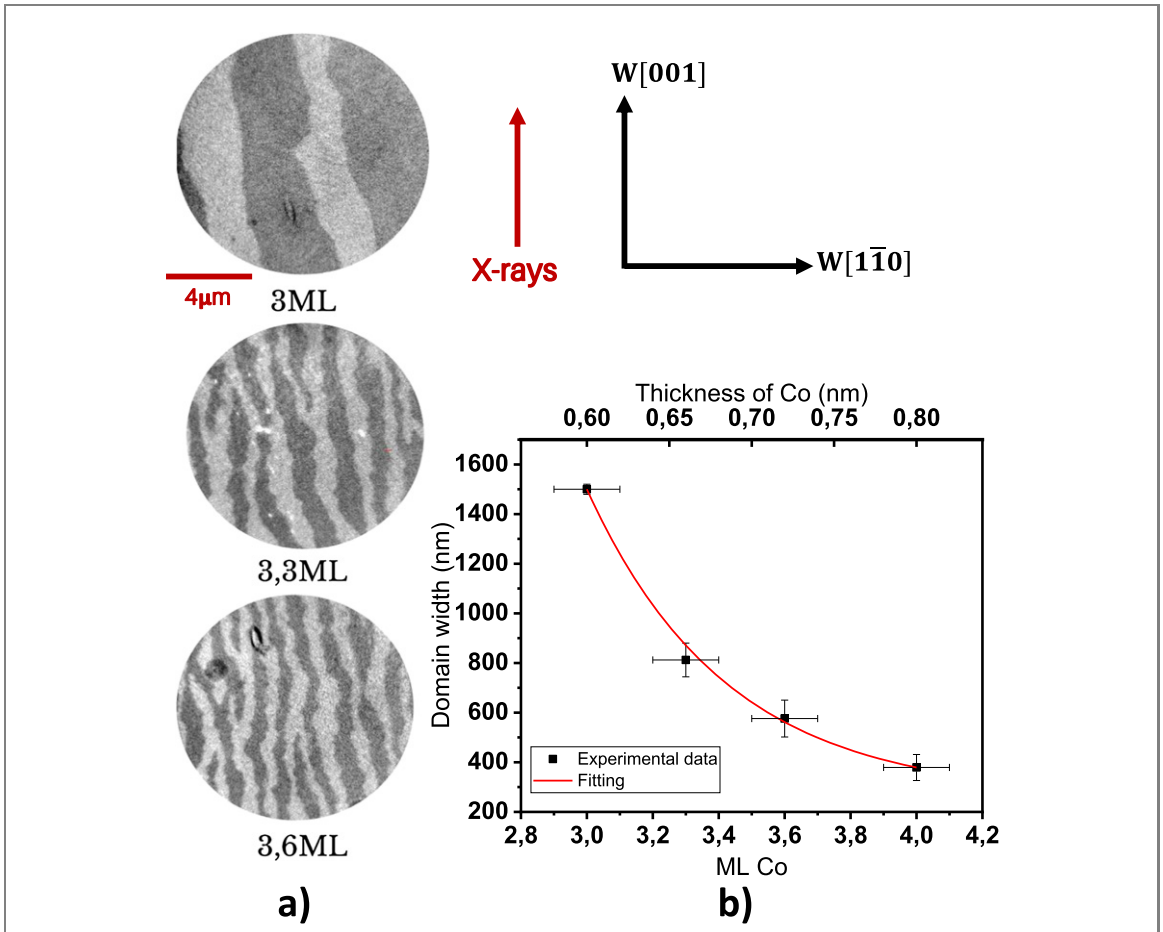

Figure 4. (a) XMCD-PEEM images, taken with the projection of the x-ray beam on the sample surface parallel to the W[001] direction, for different thicknesses of Co. The stripe domain width decreases exponentially with the Cobalt thickness as can be seen in (b). The thickness of the Co layer was determined from the position in mm on the wedge and the known thickness gradient.

energy and the domain wall energy. The experimental points in figure 4(b) are fitted with an exponential decay, in agreement with theoretical models by Kashuba and Pokrovsky [33], without considering DMI, and by Meier *et al* [34] who considered the DMI in a two-dimensional spacing model.

The images in figure 4 do not show any extra magnetic contrast at the DW. As discussed in the previous section, the expected domain wall width is larger than the spatial resolution. However, since the magnetisation in the center of the DW is expected from the 1D model to be mainly parallel to $[\bar{1}10]$ (figure 3), it is mainly perpendicular to the incoming x-ray beam and the expected magnetic contrast is in between the contrast of the two domains, and therefore indiscernible. In order to verify this, we rotated the sample by 90° so that the image in figure 5(a) was taken with the x-ray beam oriented along the W$[\bar{1}10]$ direction, for a Co thickness of about 0.8 nm. A clear extra DW contrast is now observed for DW oriented along the [001] direction, indicating that the in-plane component of the magnetisation is perpendicular to the DW direction. Moreover, the DW contrast alternates between black and white, confirming that the DWs are chiral Néel walls. A line scan along the beam direction [figure 5(c)], allows confirming the right-hand chirality of the DWs parallel to the [001] direction, in agreement with the sign of the DMI determined by BLS. From the line scan, a DW width of $\sim 52 \pm 5$ nm can be determined. This is in good agreement with the value of $\pi\Delta_y = 59$ nm obtained for the domain wall width along the easy axis from the theoretical expression in equation (4). Note that we were not able to determine the DW magnetisation for DWs oriented along the in-plane easy axis, since DW oriented along this direction are rare and always very short.

To summarise, in agreement with the 1D model the XMCD-PEEM images reveal a strongly anisotropic domain configuration, with a dominant orientation of stripe domains and DW along the [001] direction, the in-plane hard magnetisation axis. The images reveal that these DW have chiral Néel structure. The small number and short length of DW oriented along the $[\bar{1}10]$ direction did not allow confirming the dominant Bloch configuration expected for such DW. However, the strongly anisotropic domain structure is consistent with the expected difference in energy of DW oriented along the [001] and $[\bar{1}10]$ directions. Note

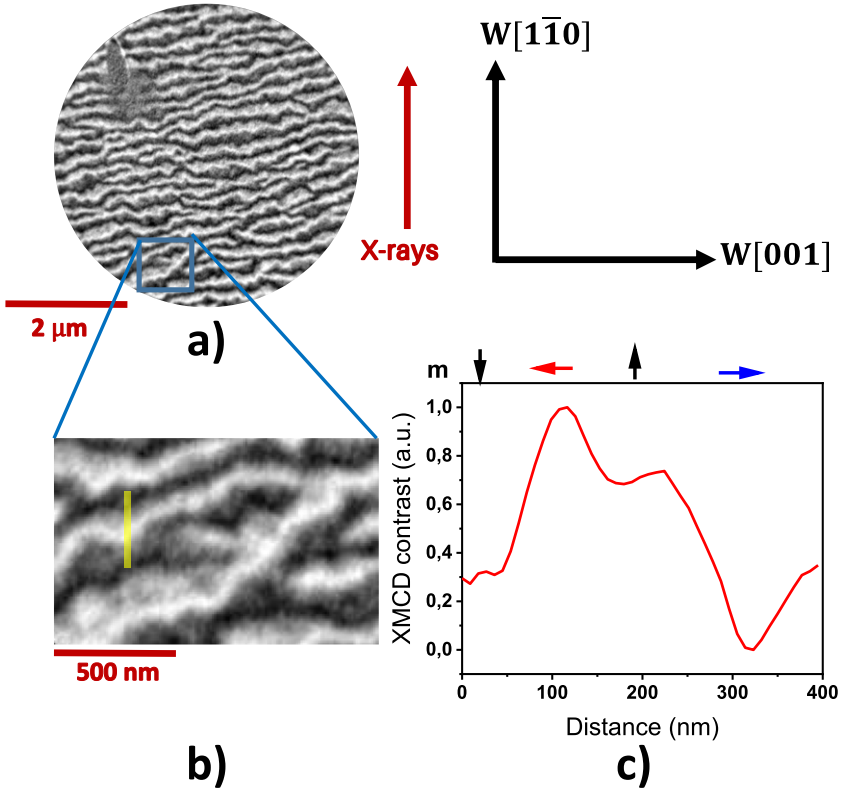

Figure 5. XMCD-PEEM images for 0.8 nm of Co with the x-rays along the W [$\bar{1}$10] direction. (a) 5 μm diameter XMCD-PEEM image (b) 1.5 × 1.5 μm^2 zoom of a part of image (a). (c) Line scan of the magnetic contrast along the direction perpendicular to the DW direction [along the yellow line in (b)].

that such a strong anisotropy of the domain wall orientation was not observed in the Fe/Ni/W(110) system of reference [16], where the value of the DMI was an order of magnitude smaller than in our case.

4.3. Anisotropic skyrmion bubbles

In this section, we discuss the effect of the anisotropic energetic environment on the stabilisation and shape of magnetic skyrmions and skyrmion bubbles. As extensively discussed in [12], a skyrmion is stabilised by DMI and exchange interactions, and its size is of the order of a few nanometers [35]. On the other hand, a skyrmion bubble is stabilised mainly by dipolar interactions and/or an external magnetic field, and its size ranges from tens of nm to a few microns. The model in reference [12] considers systems with in-plane rotational symmetry, which in our case is broken by the in-plane magnetic anisotropy. Consequently, we cannot quantitatively apply this model to estimate the equilibrium size of skyrmions and skyrmion bubbles in our system.

Skyrmion bubbles can be stabilised in thin films starting from a stripe domain phase and applying a perpendicular magnetic field [13, 36] or by the confinement in nanodots with the proper lateral size [5, 11]. We investigated the magnetic field-induced skyrmion bubbles in the region close to the spin reorientation transition (∼0.8 nm of Co), where K_{out} is small and the presence of metastable skyrmion bubbles is favored. Figure 6 shows the XMCD-PEEM images taken with the x-ray beam parallel to the W[$\bar{1}$10] direction, under the application of different out-of plane magnetic fields. Upon increasing the magnetic field strength, the width of the domains having their magnetisation anti-parallel to the field decreases in order to decrease the Zeeman energy [figure 6(b)]. For an applied field of $\mu_0 H = 11.7$ mT elliptical skyrmion bubbles are observed [figure 6(c)]. Larger applied fields caused the annihilation of the remaining bubbles and domains. Line scans of the magnetic contrast along the major and minor axes of the skyrmion bubbles give a $R_y \cong 66$ nm and $R_x \cong 23$ nm, where R_x and R_y denote the skyrmion radius along the W[$\bar{1}$10] and [001] directions, respectively.

In order to understand the role of the in-plane anisotropy on the skyrmion shape, we performed micromagnetic simulations using the code MuMax3 [37]. Since the goal was to study the influence of the DMI in the presence of the in-plane anisotropy, we performed simulations for two values of D and two values of K_{in}, fixing all the other parameters. We considered an isotropic DMI taking the highest values for Au/Co/W and for AuPt/Co/W in table 1, divided by the Co thickness of the simulation layer

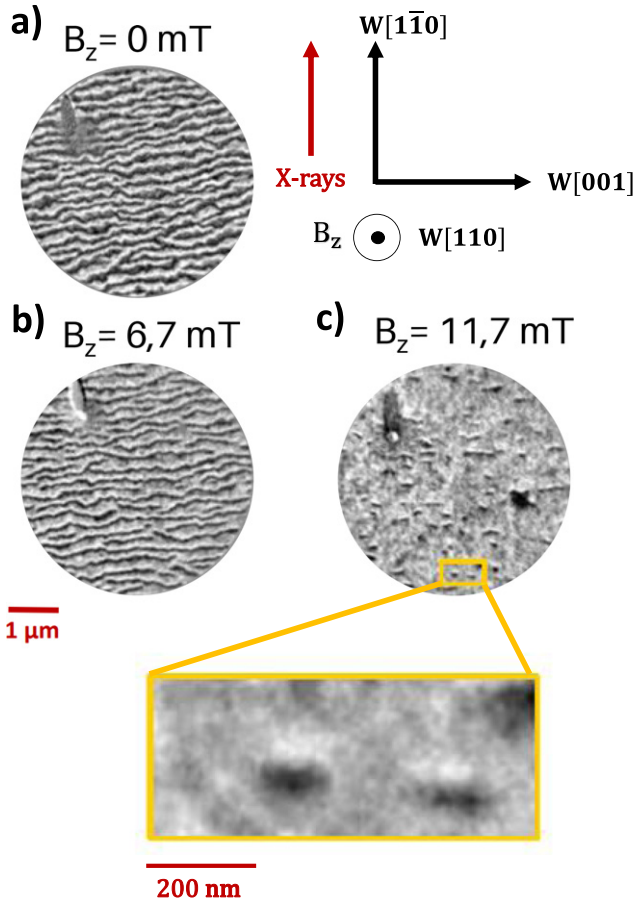

Figure 6. XMCD-PEEM images with the x-rays along W[$\bar{1}$10], at the same position but at different perpendicularly applied magnetic fields. When a magnetic field $\mu_0 H$ equal to 11.7 mT is applied elliptical skyrmion bubbles are observed.

($t_{FM} = 0.6$ nm): $D = 0.29/0.6 = 0.48$ mJ m^{-2} and $D = 0.79/0.6 = 1.32$ mJ m^{-2}. We use $A = 16$ pJ m^{-1}, $K_{out} = 0.2$ MJ m^{-3}, $M_S = 1.15$ MA m^{-1}, and in-plane anisotropy $K_{in} = 136$ kJ m^{-3}, which are the parameters found for Au/Co/W. A 60 nm diameter circular bubble domain with zero domain wall width is set in the center of the 400 nm dot and then relaxed. The results are shown in figure 7.

In the absence of in-plane magnetic anisotropy ($K_{in} = 0$) and for a small DMI value, a skyrmion bubble cannot be stabilised and therefore a uniform ferromagnetic state is obtained [figure 7(a)]. Using a larger DMI value, a skyrmion bubble can be stabilised [figure 7(b)] [5]. By adding a non-zero in-plane anisotropy that brings the system closer to an easy-plane anisotropy (i.e., $K_{out} = K_{in}$), the energy density of DW oriented along the hard in-plane axis is reduced, allowing the stabilisation of a skyrmion with a small ellipticity for a small DMI value [figure 7(c)]. The ellipticity increases upon increasing the DMI [figure 7(d)].

This elliptical shape of the skyrmion bubbles can be explained by the anisotropy of the domain wall energy as discussed before. For a given surface area, the total domain wall energy depends on the shape of the skyrmion bubble, while the surface dipolar energy and the Zeeman energy are more or less constant. The total DW energy, i.e., the DW energy density multiplied by its length, can be minimised by increasing the DW length along the in-plane hard axis and decreasing its DW length along the in-plane easy axis, leading to an elliptical skyrmion shape.

Figure 8 shows the elliptical skyrmion bubble stabilised in a 400 nm diameter dot with the experimental values of the magnetic parameters in table 1 for AuPt/Co/W. The best agreement with the experiment is found for an applied magnetic field $B_z = 5$ mT, giving $R_y \cong 65$ nm and $R_x \cong 36$ nm. The magnetic field is smaller than in the experiment ($B_z = 11.7$ mT), but we consider that the agreement is good since the skyrmion size is very sensitive to the magnetic parameters. Also, the experiment is performed in a continuous film, while the simulations are for a circular dot, where the dipolar effects are modified.

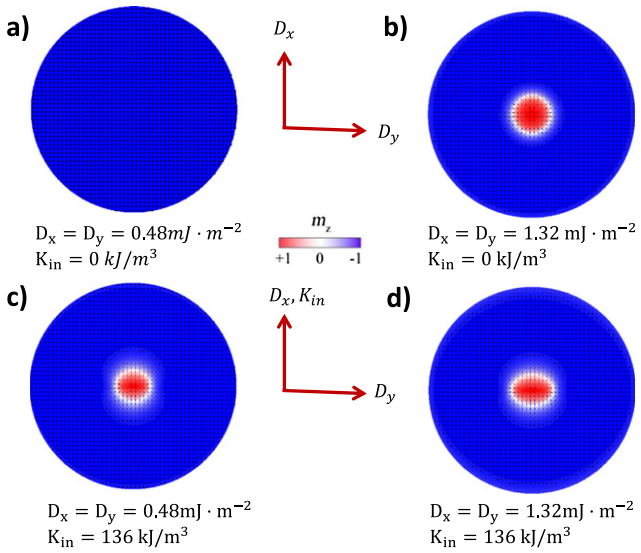

Figure 7. Micromagnetic simulations with $K_{out} = 0.2$ mJ m^{-2}, $A = 16$ pJ m^{-1}, $M_s = 1.15$ MA m^{-1} in a 400 nm diameter circular nanodot (a) $D_x = D_y = 0.48$ mJ m^{-2}, $K_{in} = 0$ kJ m^{-3} (b) $D_x = D_y = 1.32$ mJ m^{-2}, $K_{in} = 0$ kJ m^{-3}, (c) $D_x = D_y = 0.48$ mJ m^{-2}, $K_{in} = 136$ kJ m^{-3}, (d) $D_x = D_y = 1.32$ mJ m^{-2}, $K_{in} = 136$ kJ m^{-3}.

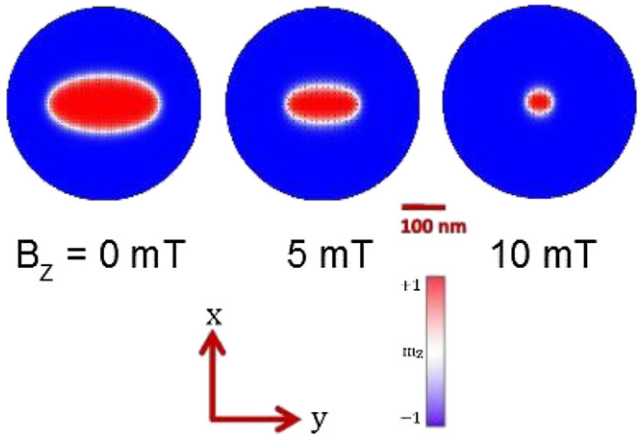

Figure 8. Micromagnetic simulations with experimental values of the magnetic parameters reported in table 1 for AuPt/Co/W, for applied perpendicular magnetic fields of $B_z = 0$ mT, 5 mT and 10 mT.

5. Conclusions

We studied the relationship between the symmetry of the crystal and its magnetic properties, and their influence on the shape of domains and skyrmion bubbles, in an epitaxial perpendicularly magnetised AuPt/Co/W(110) system. The interplay between the in-plane anisotropy and the DMI in this system results in a strong dependence of the energy of DW on their orientation with respect to the crystallographic axes. This anisotropic behavior leads to a spontaneous orientation of magnetic stripe domains along the hard in-plane axis. The application of a weak perpendicular magnetic field leads to the transformation of the magnetic stripe domains into skyrmion bubbles with an elliptical shape and a size of about 100 nm. This elliptical shape, due to the anisotropic domain wall energy, is in good agreement with micromagnetic simulations. The anisotropic shape of the skyrmion bubbles can be expected to lead to strongly anisotropic dynamic properties, both in the breathing mode [38] and when driven by spin-polarised currents [39].

Acknowledgments

JPG acknowledges a PhD Grant from GRECQUE and the Laboratoire d'excellence LANEF (Grant No. ANR-10-LABX-51-01). LC, JPG, SP and JV acknowledge financial support of the Agence Nationale de la

Recherche, project ANR-17-CE24-0025 (TOPSKY). We also acknowledge financial support from the DARPA TEE program through Grants No. MIPR HR001183155 (SP and JV) and R18-687-0004 (JMS and HTN). We thank V Guisset and P David for their help with sample preparation.

Data availability statement

The data that support the findings of this study are available upon reasonable request from the authors.

ORCID iDs

Lorenzo Camosi https://orcid.org/0000-0002-1564-8278
Jose Peña Garcia https://orcid.org/0000-0002-1801-8108
Olivier Fruchart https://orcid.org/0000-0001-7717-5229
Stefania Pizzini https://orcid.org/0000-0002-7016-1083
Andrea Locatelli https://orcid.org/0000-0002-8072-7343
Tevfik Onur Menteş https://orcid.org/0000-0003-0413-9272
Francesca Genuzio https://orcid.org/0000-0003-0699-2525
Justin M Shaw https://orcid.org/0000-0003-2027-1521
Jan Vogel https://orcid.org/0000-0001-8008-6980

References

[1] Fert A, Cros V and Sampaio J 2013 *Nat. Nanotechnol.* **8** 152
[2] Dzyaloshinsky I 1958 *J. Phys. Chem. Solids* **4** 241–55
[3] Moriya T 1960 *Phys. Rev.* **120** 91
[4] Thiaville A, Rohart S, Jué É, Cros V and Fert A 2012 *Europhys. Lett.* **100** 57002
[5] Rohart S and Thiaville A 2013 *Phys. Rev.* B **88** 184422
[6] Bogdanov A and Rößler U 2001 *Phys. Rev. Lett.* **87** 037203
[7] Roessler U K, Bogdanov A N and Pfleiderer C 2006 *Nature* **442** 797
[8] Mühlbauer S, Binz B, Jonietz F, Pfleiderer C, Rosch A, Neubauer A, Georgii R and Böni P 2009 *Science* **323** 915
[9] Romming N, Hanneken C, Menzel M, Bickel J E, Wolter B, von Bergmann K, Kubetzka A and Wiesendanger R 2013 *Science* **341** 636
[10] Moreau-Luchaire C *et al* 2016 *Nat. Nanotechnol.* **11** 444
[11] Boulle O *et al* 2016 *Nat. Nanotechnol.* **11** 449
[12] Bernand-Mantel A, Camosi L, Wartelle A, Rougemaille N, Darques M and Ranno L 2018 *SciPost Phys.* **4** 27
[13] Jiang W *et al* 2015 *Science* **349** 283
[14] Woo S *et al* 2016 *Nat. Mater.* **15** 501
[15] Bogdanov A and Yablonski D 1989 *Zh. Eksp. Teor. Fiz.* **95** 178
[16] Chen G, N'Diaye A T, Kang S P, Kwon H Y, Won C, Wu Y, Qiu Z Q and Schmid A K 2015 *Nat. Commun.* **6** 6598
[17] Chen G, Mascaraque A, N'Diaye A T and Schmid A K 2015 *Appl. Phys. Lett.* **106** 242404
[18] Fritzsche H, Kohlhepp J and Gradmann U 1995 *Phys. Rev.* B **51** 15933
[19] Hoffmann M, Zimmermann B, Müller G, Schürhoff D, Kiselev N, Melcher C and Blügel S 2017 *Nat. Commun.* **8** 308
[20] Camosi L *et al* 2017 *Phys. Rev.* B **95** 214422
[21] Nishiyama Z 1934 *Sci. Rep. Tohoku Univ.* **23** 637
[22] Wassermann G 1933 *Archiv für das Eisenhüttenwesen* **6** 347–51
[23] Fruchart O, Rousseau A, Schmaus D, L'Hoir A, Haettel R and Ortega L 2011 *Appl. Phys. Lett.* **98** 131906
[24] Cahn 1991 *Advanced Materials* **3** 628–9
[25] Damon R and Eshbach J 1961 *J. Phys. Chem. Solids* **19** 308
[26] Zakeri K, Zhang Y, Prokop J, Chuang T-H, Sakr N, Tang W and Kirschner J 2010 *Phys. Rev. Lett.* **104** 137203
[27] Di K, Zhang V L, Lim H S, Ng S C, Kuok M H, Yu J, Yoon J, Qiu X and Yang H 2015 *Phys. Rev. Lett.* **114** 047201
[28] Nembach H T, Shaw J M, Weiler M, Jue E and Silva T J 2015 *Nat. Phys.* **11** 825
[29] Stashkevich A, Belmeguenai M, Roussigné Y, Cherif S, Kostylev M, Gabor M, Lacour D, Tiusan C and Hehn M 2015 *Phys. Rev.* B **91** 214409
[30] Ajejas F, Křižáková V, de Souza Chaves D, Vogel J, Perna P, Guerrero R, Gudin A, Camarero J and Pizzini S 2017 *Appl. Phys. Lett.* **111** 202402
[31] Ma X, Yu G, Tang C, Li X, He C, Shi J, Wang K L and Li X 2018 *Phys. Rev. Lett.* **120** 157204
[32] Metaxas P J, Jamet J P, Mougin A, Cormier M, Ferré J, Baltz V, Rodmacq B, Diény B and Stamps R L 2007 *Phys. Rev. Lett.* **99** 217208
[33] Kashuba A and Pokrovsky V L 1993 *Phys. Rev.* B **48** 10335
[34] Meier T, Kronseder M and Back C 2017 *Phys. Rev.* B **96** 144408
[35] Heinze S, von Bergmann K, Menzel M, Brede J, Kubetzka A, Wiesendanger R, Bihlmayer G and Bluegel S 2011 *Nat. Phys.* **7** 713
[36] Juge R *et al* 2018 *J. Magn. Magn. Mater.* **455** 3
[37] Vansteenkiste A, Leliaert J, Dvornik M, Helsen M, Garcia-Sanchez F and Van Waeyenberge B 2014 *AIP Adv.* **4** 107133
[38] Kim J-V, Garcia-Sanchez F, Sampaio J, Moreau-Luchaire C, Cros V and Fert A 2014 *Phys. Rev.* B **90** 064410
[39] Xia J, Zhang X, Ezawa M, Shao Q, Liu X and Zhou Y 2020 *Appl. Phys. Lett.* **116** 022407